ANNALS OF GEOPHYSICS, 69, 2026; doi:10.4401/ag-9577
OPEN ACCESS

Crustal Thickness and Vp/Vs Variations Beneath the Karlıova Triple Junction (Eastern Anatolia-Türkiye) Revealed by Receiver Function Analysis

Tuğçe Ergün[*,1]

[(1)] Boğaziçi University, Kandilli Observatory and Earthquake Research Institute, Regional Earthquake-Tsunami Monitoring Center, İstanbul, Türkiye

Article history: received April 10, 2026; accepted July 7, 2026

Abstract

Eastern Anatolia is one of the most tectonically active regions of the Alpine-Himalayan orogenic belt, shaped by the ongoing Arabia-Eurasia continental collision and major strike-slip fault systems. In this study, we constrain the crustal structure beneath the Karlıova Triple Junction-Bingöl region using teleseismic receiver function analysis combined with H-κ stacking. We analyze a high-quality and long-term dataset recorded by permanent broadband seismic stations of the Kandilli Observatory and Earthquake Research Institute, using teleseismic earthquakes with Mw ≥ 6.2 selected from an initial larger dataset and epicentral distances of 30°-95°. The results reveal strong lateral variations in crustal thickness, with Moho depths ranging from ~30 km to ~47 km. Stations located along major active fault zones generally exhibit thicker crust. Average crustal Vp/Vs ratios vary between 1.64 and 1.95, indicating significant heterogeneity in crustal elastic properties. Clear Ps conversions and well-developed crustal multiples confirm the robustness of the results, while additional early arrivals at several stations suggest internal crustal complexity. The observed patterns are consistent with geophysical and geodynamic models suggesting a hot, thinned, and relatively low-density lithosphere beneath Eastern Anatolia. These results provide a consistent basis for interpreting lithospheric deformation and the relationship between crustal structure and major fault systems in Eastern Anatolia.

Keywords: Eastern Anatolia; Receiver Functions; Crustal Thickness; Moho Depth; Vp/Vs ratio

1. Introduction

Eastern Anatolia represents one of the most tectonically active and geodynamically complex regions of the Alpine-Himalayan orogenic belt. The region forms a highly deformed plateau with an average elevation of approximately 2 km resulting from the ongoing continent-continent collision between the Arabian and Eurasian plates. This convergence zone is bounded by major lithospheric-scale tectonic structures, including the left-lateral East Anatolian Fault Zone (EAFZ), the right-lateral North Anatolian Fault Zone (NAFZ) and the Bitlis-Zagros Fold and Thrust Belt (BZFTB) (Fig. 1). Geological, geodetic and geophysical observations indicate that both the NAFZ and EAFZ have been active since at least the Miocene, accommodating relative plate motions through large-scale strike-slip deformation (Barka and Kadinsky-Cade, 1988; Bozkurt, 2001). The northward motion of the Arabian Plate relative to Eurasia drives the westward extrusion of the Anatolian microplate primarily accommodated by right-lateral motion along the NAFZ (Şengör, 1979; McClusky et al., 2000; Le Pichon et al., 2015) and left-lateral motion along the EAFZ (McKenzie, 1972; Jackson and McKenzie, 1988), in conjunction with southwest rollback of the Hellenic subduction system (Jolivet and Faccenna, 2000). Deformation is further transferred northward into the Lesser and Greater Caucasus, where thrusting and strike-slip faulting partially compensate the ongoing Arabia-Eurasia convergence (Philip et al., 1989). This continental collision is also expressed by widespread Neogene-Quaternary volcanism, which intensified during the Late Miocene and originated from the lower lithospheric mantle, potentially related to lithospheric thinning or delamination processes (Pearce et al., 1990; Keskin, 2003).

Seismological investigations provide strong evidence for anomalous lithospheric and upper-mantle structure beneath Eastern Anatolia. Pn-wave tomography (Al-Lazki et al., 2003), Sn-wave attenuation (Gök et al., 2003), joint inversions of surface waves and receiver functions (Angus et al., 2006; Gök et al., 2007) and shear-wave splitting analyses (Sandvol et al., 2003) consistently indicate a markedly thinned or absent mantle lithosphere beneath the Anatolian Plateau. Receiver function studies reveal pronounced crustal thickening, with Moho depths locally exceeding ~45 km and exhibiting sharp lateral variations near plateau margins and major fault zones. These variations correlate well with surface topography, regional uplift and elevated crustal Vp/Vs ratios, suggesting significant thermal and compositional heterogeneity within the crust (Eken et al., 2021; Ogden and Bastow, 2022; van Hinsbergen et al., 2024). Collectively, these observations support models invoking dynamic mantle support for the East Anatolian Plateau (Zor et al., 2003; Faccenna and Becker, 2010; Karabulut et al., 2019).

A key structural element within this tectonic framework is the Karlıova Triple Junction (KTJ), a major pull-apart basin located at the intersection of the NAFZ and EAFZ (Figs. 1 and 2). The KTJ is a zone of concentrated strain accumulation and complex fault interactions, producing a highly heterogeneous deformation field with important implications for earthquake nucleation and seismic hazard (Medved et al., 2021; Cheloni et al., 2025). East of the KTJ, deformation within the East Anatolian Plateau is distributed across a network of NW- and NE-trending active strike-slip faults, indicating significant internal strain accommodation rather than rigid block motion. Geodetic observations further highlight strong spatial variations in deformation across the KTJ. Early GPS studies (Reilinger et al., 1997; Reilinger et al., 2006; McClusky et al., 2000) demonstrated that the western and eastern parts of the junction deform in different ways: crustal shortening dominates approximately 150 km north of the BZFTB in the east, whereas westward escape tectonics is the driving force in the west. Recent GNSS-based studies reveal significant interseismic coupling and horizontal displacements in the Karlıova region, consistent with active strain accumulation within the brittle crust (Liu et al., 2025; Cheloni et al., 2025). At a broader scale, updated GNSS velocity fields for southeastern Türkiye and Cyprus show that Arabia-Anatolia relative motion is distributed across a ~50-60 km-wide shear zone, rather than being confined to a single fault trace, with slip rates of ~5-6 mm/yr along the EAFZ and substantial deformation accommodated by secondary fault systems (Özbey et al., 2024).

Instrumental seismicity since the early 20th century highlights persistent moderate-to-large earthquakes concentrated along the EAFZ and its segments, reflecting ongoing strain accumulation and release. Significant events include the 1939 Erzincan (Mw 7.9), 1971 Bingöl (Mw 6.9), 2003 Bingöl (Mw 6.4), 2010 Elazığ (Mw 6.1), 2020 Sivrice (Mw 6.8) and the catastrophic 2023 Kahramanmaraş earthquake sequence (Mw 7.8 and Mw 7.6), which produced extensive surface ruptures, exceptionally high coseismic slip and widespread damage (Tan et al., 2011; Beltrán et al., 2020; Konca et al., 2021; Wang and Barbot, 2024; Karabulut et al., 2023; He et al., 2023; Güvercin 2024; Liu et al., 2025). Focal mechanism solutions, stress field analyses, rupture characteristics and aftershock distributions consistently indicate predominantly shallow strike-slip faulting within a seismogenic zone of ~15 km thickness, in agreement with the regional tectonic regime (Güvercin et al., 2022; Güvercin, 2023; Colavitti et al., 2025). The distribution of seismicity (Fig. 2) provides tectonic context for the receiver function analysis and illustrates the active deformation patterns within the KTJ, where seismicity is predominantly confined to the upper crust above the estimated Moho depths, suggesting that most deformation is accommodated within the brittle crust.

Historical earthquake records further demonstrate that the EAFZ has repeatedly generated destructive earthquakes over the past several centuries, including major events in 1789, 1795, 1866, 1872-1875, and 1893 (Ambraseys and Jackson, 1998). These observations, supported by paleoseismological trenching studies, estimate long recurrence intervals for large earthquakes and confirm the fault's capacity to produce Mw ≥ 7 events (Bayrak et al., 2015; Gülerce et al., 2017). The complex triple-junction geometry enhances stress transfer between adjacent fault segments and may promote the development of seismic gaps capable of generating future large earthquakes (Bektaş et al., 2025).

Seismic tomography beneath Eastern Anatolia further reveals strong lateral and vertical velocity contrasts interpreted as reflecting accreted terranes, dipping fault zones, thickened crust beneath the plateau and sedimentary basins, all of which significantly influence seismic wave propagation and ground-motion patterns in the Karlıova region (Medved et al., 2021; Güvercin, 2023).

In this study, we investigate the crustal structure and Moho topography beneath the KTJ Bingöl region using teleseismic receiver function analysis and H-κ stacking. Previous receiver function studies in Eastern Anatolia have provided important constraints on crustal thickness and Moho depth; however, these results are often derived from heterogeneous datasets, time periods, and processing strategies, which limit their direct comparability across different stations and tectonic domains. We use long-term continuous observations from the Kandilli Observatory Earthquake Research Institute (KOERI) broadband seismic network and apply a uniform receiver function computation and H-κ stacking workflow to all stations. This approach enables a systematic and internally consistent evaluation of crustal thickness and Vp/Vs variability across the study region, providing a clearer characterization of lateral variations in crustal properties and their relationship to major fault systems and tectonic processes in Eastern Anatolia.

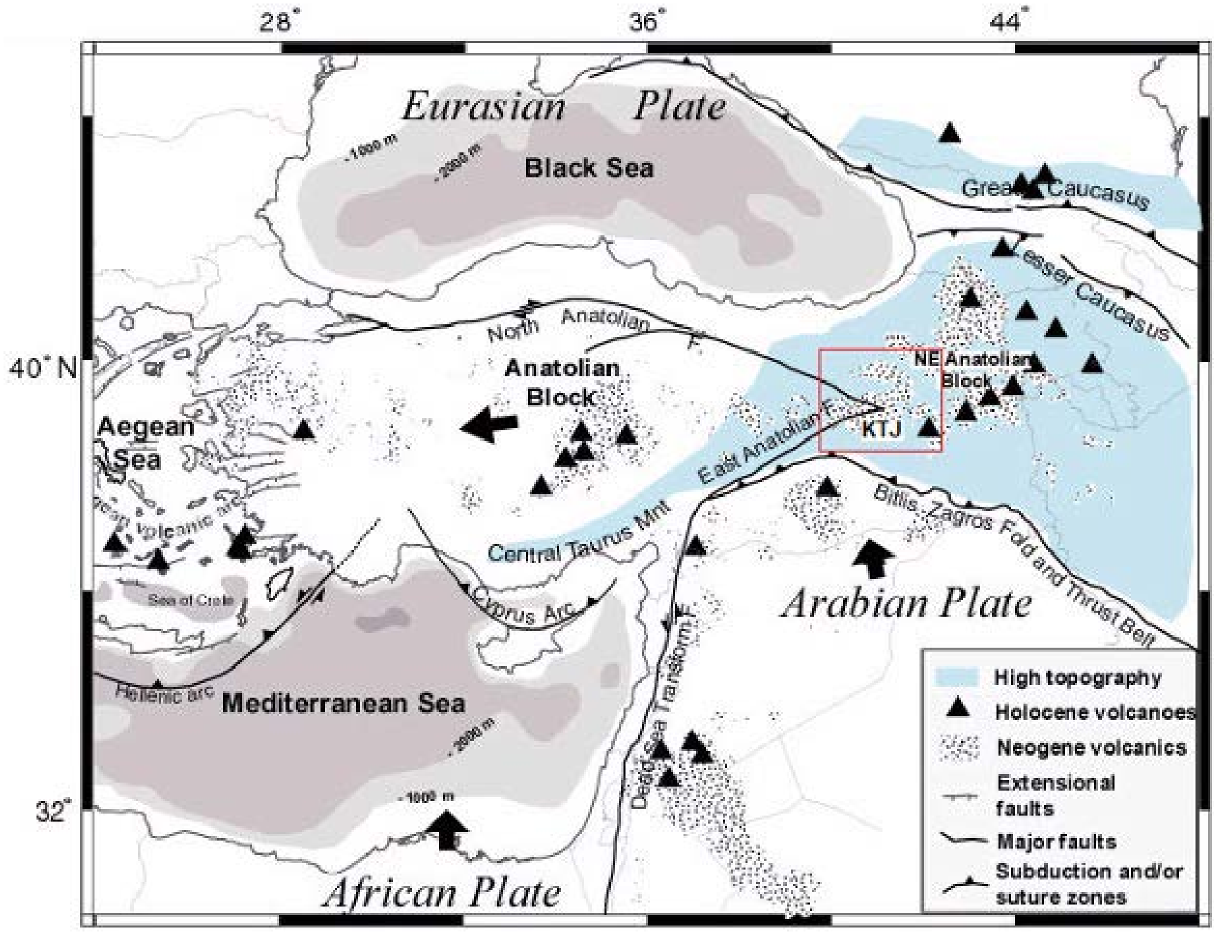

Figure 1. Simplified tectonic map of Türkiye and its near vicinity (modified from Barka and Reilinger, 1997). Main tectonic features are explained in the inset. KTJ: Karlıova Triple Junction. The study area is marked by the red rectangle. Black arrows indicate plate motions. Simplified bathymetric contours are also plotted in 1000 m intervals.

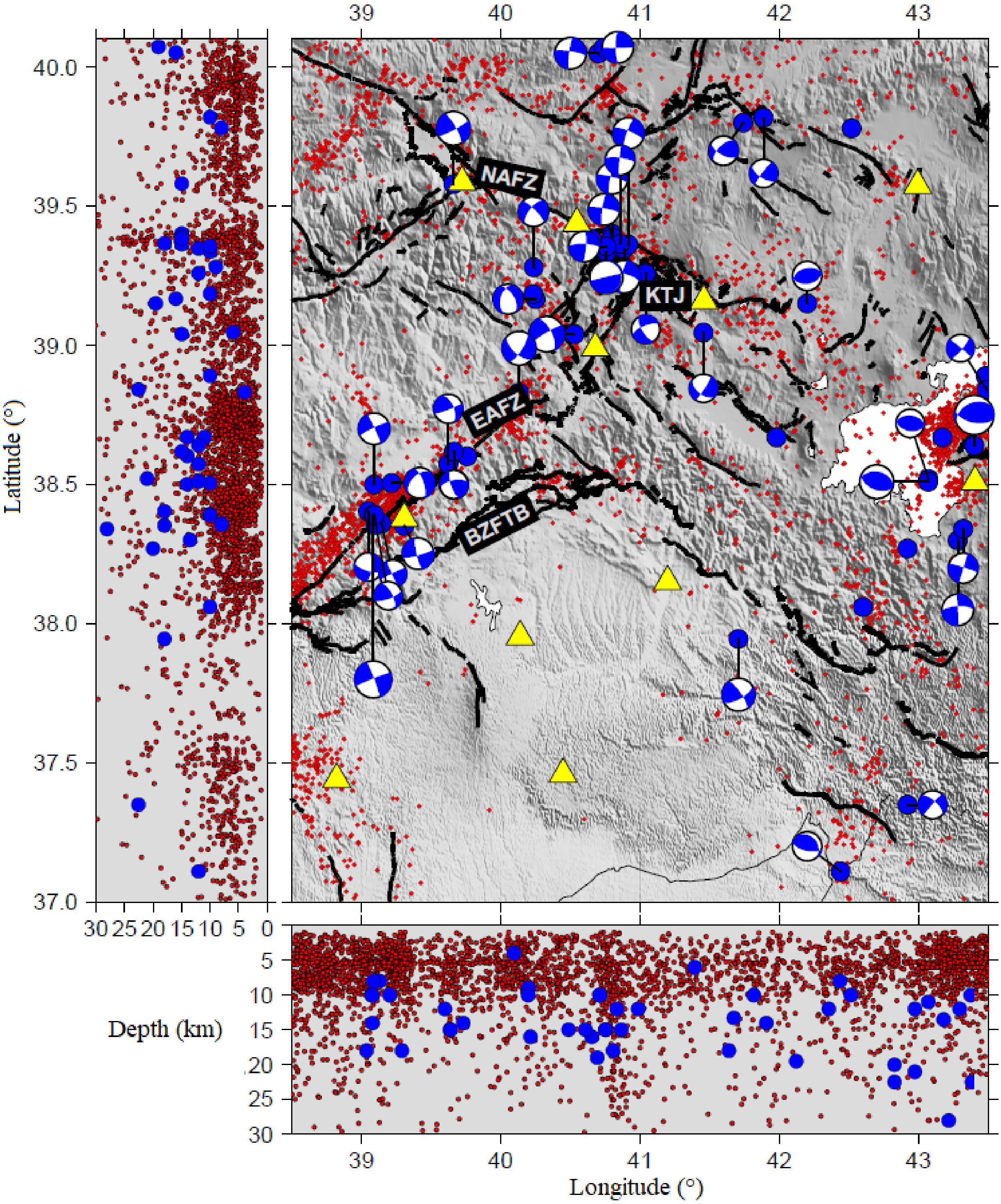

Figure 2. Seismicity of the KTJ and its surroundings (2005-present), based on the earthquake catalogue of the Boğaziçi University KOERI. Major active faults are shown as solid black lines. Earthquakes with magnitudes M ≥ 3.0 are indicated by red circles, while focal mechanism solutions (compiled from the Harvard CMT and KOERI catalogues) are shown for events with magnitudes M ≥ 4.5 (beachball size scaled by magnitude). Broadband seismic stations are represented by yellow triangles. Depth distribution of earthquakes is also shown by latitude and longitude cross sections. Abbreviations: NAFZ – North Anatolian Fault Zone; EAFZ – East Anatolian Fault Zone; KTJ – Karlıova Triple Junction; BZFTB – Bitlis-Zagros Fold and Thrust Belt.

2. Data and Methods

To investigate the crustal thickness beneath Eastern Anatolia, this study analyzed three-component waveform data recorded by permanent broadband seismic stations operated by the KOERI (Fig. 2). The network consists of broadband sensors with corner periods ranging between 30 s and 120 s, providing high-quality recordings suitable for teleseismic receiver function analysis. The initial data set comprised teleseismic earthquakes with moment magnitudes greater than Mw 5.5, recorded between 2007 and 2025. Owing to the large volume of available teleseismic data and to ensure consistently high signal-to-noise ratios across all stations, we adopted a higher magnitude threshold (Mw ≥ 6.2) for the final dataset. Larger-magnitude events provide clearer P-wave onsets and more stable P-to-S converted phases. These are essential for the reliable identification of Moho conversions and their multiples, particularly in a tectonically complex region such as Eastern Anatolia. Furthermore, the use of higher-magnitude events minimizes uncertainties related to noise contamination, site effects, and variations in instrument performance, thereby improving the robustness of the H-κ stacking results.

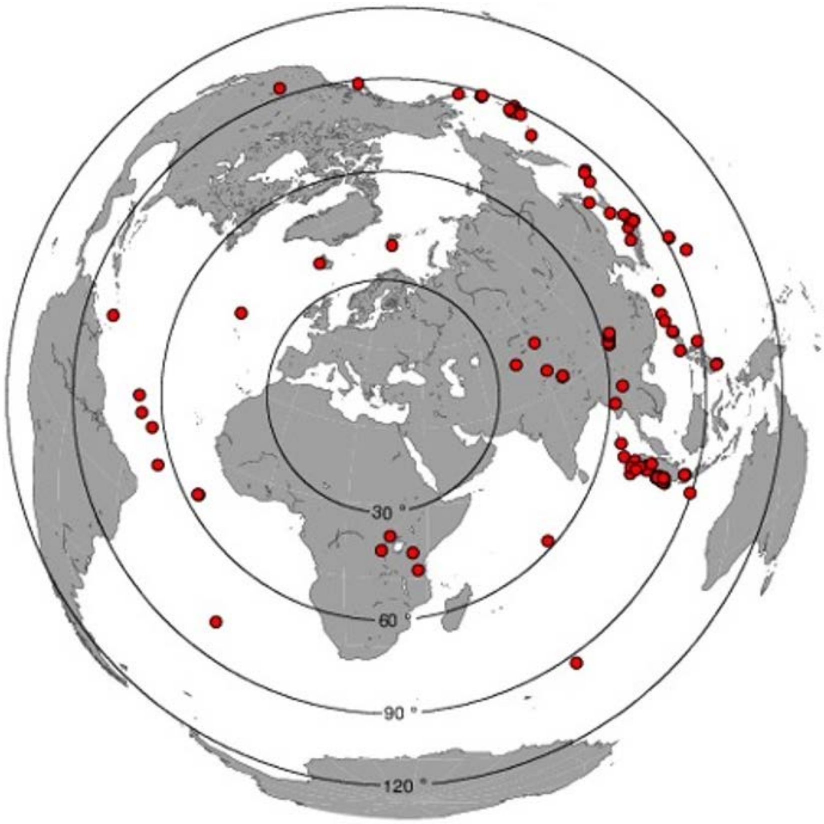

Figure 3. Equidistant projection of teleseismic earthquakes (Mw ≥ 6.2) used for the receiver function analysis, selected within epicentral distances of 30°-95°. The distribution provides sufficient azimuthal coverage for robust H-κ stacking.

Teleseismic distances were restricted to the range of 30°-95°. Events at distances shorter than 30° were excluded due to complications arising from upper-mantle triplication and complex travel-path effects, whereas distances greater than approximately 95° were avoided because the stations fall within the P-wave shadow zone. All selected events were visually inspected and waveforms with clear P-wave onsets and high signal-to-noise ratios were retained. The number of receiver functions varies among stations after quality control, ranging approximately between 130 and 180, depending on data availability and station performance. The azimuthal distribution of these events is non-uniform, with the majority originating from subduction zones in the Western Pacific, and fewer events from the Indian and Atlantic Oceans (Fig. 3). Despite this disparity, the overall azimuthal coverage is sufficient to provide robust constraints on crustal structure beneath the study area. Data quality and quantity vary among stations due to occasional instrument malfunctions and differences in local noise conditions. In particular, stations located above thick sedimentary basins generally exhibit lower signal-to-noise ratios compared to those installed on crystalline or volcanic basement, reflecting the influence of near-surface geology on seismic recordings.

Receiver functions were computed using the time-domain iterative deconvolution method of Ligorría and Ammon (1999). Prior to deconvolution, three-component seismograms were rotated from the Z-N-E coordinate system into the local Z-R-T ray-based coordinate system, isolating the P-to-S converted phases on the radial component. The vertical component was deconvolved from the radial component to remove the earthquake source signature and the propagation effects along the path from the source to beneath the recording station. A Gaussian filter with an "α" parameter of 4.5 was applied to suppress high-frequency noise while preserving converted phase energy. Both radial and transverse receiver functions were visually inspected by sorting them according to back-azimuth and epicentral distance. Receiver functions exhibiting anomalous amplitudes or unstable waveforms were excluded from further analysis.

Crustal thickness (H) and Vp/Vs ratio (κ) beneath each station were estimated using the H-κ stacking technique of Zhu and Kanamori (2000). For the stacking analysis, a constant crustal P-wave velocity of 6.3 km/s was assumed, because this value is widely used as a representative average crustal velocity in receiver-function studies and serves as a reasonable first-order approximation where station-specific crustal velocity information is unavailable. Although variations in Vp may affect the absolute values of H and Vp/Vs, the first-order results remain generally robust within reasonable bounds of Vp variation. The most prominent signal following the direct P arrival on the radial receiver function is the P-to-S converted phase (Ps) generated at the Moho discontinuity. The time delay between the Ps and direct P phases is proportional to crustal thickness and the average seismic velocity structure above the Moho. Since the differential travel time between S and P waves is used, crustal thickness estimates are only weakly sensitive to absolute P-wave velocity, but depend more strongly on the crustal Vp/Vs ratio. This trade-off between H and κ can be significantly reduced by incorporating crustal multiples, namely PpPs and PsPs + PpSs phases. Including these multiples provides additional constraints on the depth of the Moho and the average Poisson's ratio of the crust. Receiver functions were stacked over a grid of crustal thicknesses and Vp/Vs ratios using unequal weights of 0.7, 0.2, and 0.1 for the Ps, PpPs, and PsPs + PpSs phases, respectively. This stacking algorithm transforms receiver functions directly from the time domain into the H-κ domain without the need for manual phase picking. Constructive interference of the primary conversion and its multiples maximizes the stack amplitude, yielding the optimal H-κ solution. The resulting Vp/Vs ratios represent average values for the entire crust, from the surface to the Moho, and provide first-order constraints on crustal composition and physical state beneath Eastern Anatolia. Uncertainties in H and Vp/Vs were estimated from the width of the closed high-amplitude region surrounding the maximum in the H-κ stacking domain. Specifically, the uncertainty bounds were approximated from the half-width of the principal closed contour around the best-fitting solution along the Moho-depth and Vp/Vs axes, respectively. Stations with compact and well-focused maxima yield lower uncertainties, whereas broader or elongated maxima indicate increased uncertainty.

3. Results

Receiver function analysis and H-κ stacking were applied to the broadband seismic stations listed in Table 1, providing robust estimates of crustal thickness (H) and average crustal Vp/Vs ratios beneath Eastern Anatolia. Crustal thickness values range from approximately 30 km to 47 km, indicating pronounced lateral variations in Moho depth across the study area. The thinnest crust is observed beneath station MAZI (~30 km), whereas the thickest crust is detected beneath VANB (~47 km).

Stations located along or in close proximity to major active fault systems, including VRTB, YEDI, and ERZN, consistently exhibit relatively thicker crust (generally ~39-42 km), while stations located away from major fault structures show a comparatively thinner crust. These observations highlight strong spatial heterogeneity in Moho topography across the KTJ-Bingöl region. Crustal Vp/Vs ratios vary between 1.64 and 1.95 (Table 1). Lower values (≤1.70) are observed at BNGB, DYBB, SVAN and URFA, whereas higher values (>1.90) are obtained at SVRC and VRTB. The highest Vp/Vs ratio (~1.95) is observed at station VRTB, indicating significant lateral variations in crustal elastic properties

Representative H-κ stacking results are shown in Figs. 4 and 5 for stations BNGB and ERZN, respectively. At station BNGB, the Ps converted phase is clearly observed at approximately 4.5-5.0 s after the direct P-wave arrival, together with well-developed crustal multiples (PpPs and PsPs + PpSs), yielding an optimal crustal thickness of

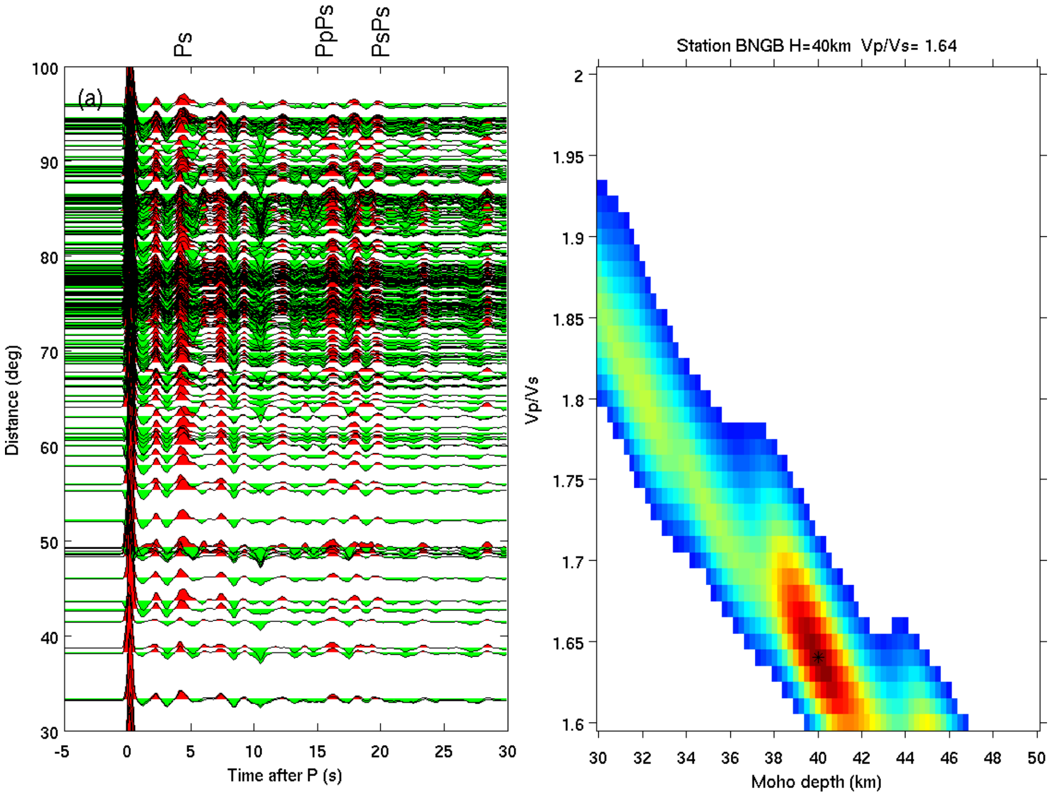

Figure 4. Radial receiver functions at station BNGB, sorted by epicentral distance, together with the corresponding H-κ stacking result. The Ps converted phase and well-developed crustal multiples (PpPs and PsPs + PpSs) are clearly identified, yielding an estimated crustal thickness of ∼40 km and a Vp/Vs ratio of ∼1.64.

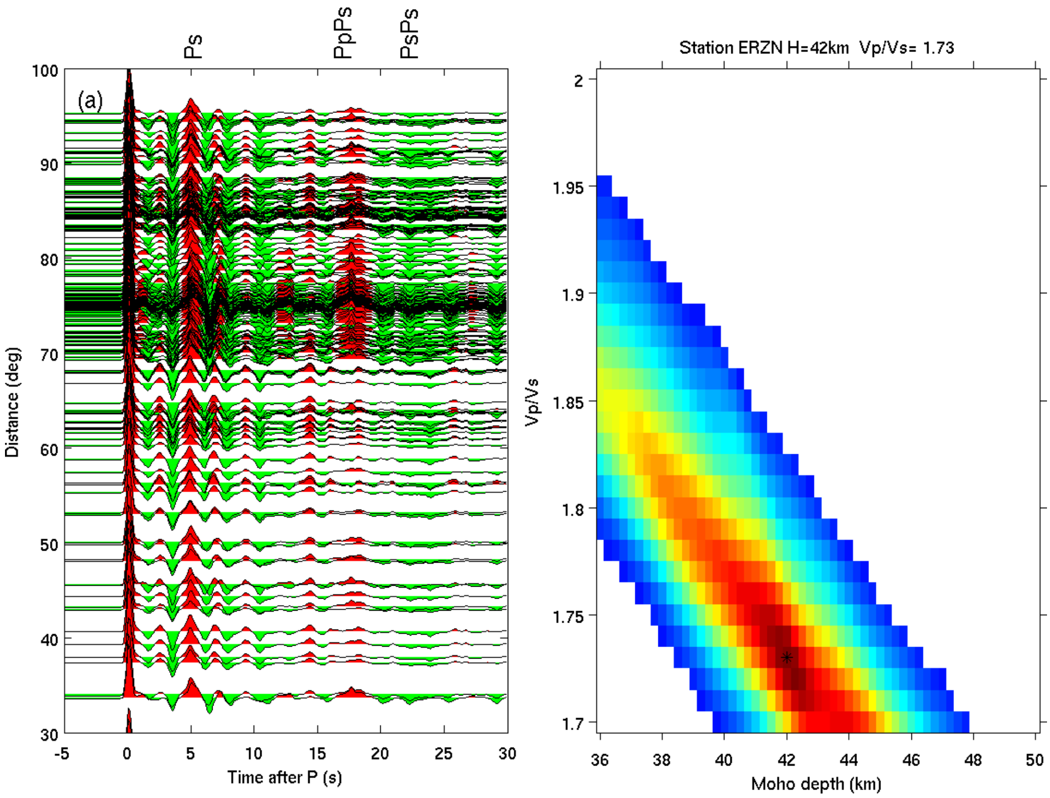

Figure 5. Radial receiver functions at station ERZN, sorted by epicentral distance, together with the corresponding H-κ stacking result. Clear Ps and multiple phases indicate a crustal thickness of ∼42 km and a Vp/Vs ratio of ∼1.73.

~40 km and a Vp/Vs ratio of ~1.64. In contrast, station ERZN, located directly on an active fault segment, exhibits a thicker crust (~42 km) and a moderately elevated Vp/Vs ratio (~1.73), with more complex waveform characteristics observed in the radial receiver functions. H-κ stack figures for all analyzed stations (Table 1) are provided in the Supplementary Material.

Stations VANB and AGRB display consistent and well-resolved H-κ stacking results. At VANB (Fig. 6), a large number of high-quality receiver functions produces a high-energy stacking pattern with a moderately broadened maximum, indicating a robust crustal thickness estimate (~47 km) with slightly increased uncertainty in Vp/Vs (~1.80). Radial receiver functions show a clear Moho conversion (Ps phase) at approximately 5-6 s, although not sharply defined and no strong evidence for distinct intracrustal discontinuities. In contrast, AGRB exhibits a more compact and well-focused stacking maximum, with a clear Ps phase at ~4.5-5.0 s and visible crustal multiples, indicating a well-constrained crustal thickness (~44 km) and relatively homogeneous crustal properties.

In addition to the representative stations shown in Figs. 4, 5 and 6, several stations not illustrated with H-κ stack figures exhibit noteworthy receiver-function characteristics. H-κ stacking figures for all stations not shown in the main text are included in the Supplementary Material.

Several stations exhibit distinctive receiver-function characteristics. At station SVRC, radial receiver functions display a pronounced Ps phase accompanied by strong crustal multiples, consistent with the high Vp/Vs ratio (~1.94) and a crustal thickness of approximately 37 km. Station VRTB similarly shows well-developed Ps and multiple phases, yielding a crustal thickness of ~39 km and a high Vp/Vs ratio (~1.95). Station YEDI shows a clear Ps phase together with additional earlier arrivals (~2-3 s), suggesting the presence of mid-crustal velocity contrasts. Similar but less pronounced features are observed at DYBB and SVAN. In contrast, station URFA exhibits a clear Ps phase but relatively weak multiples, indicating reduced impedance contrasts within the crust.

Station YEDI, located near a major fault segment, exhibits a relatively thick crust (~40 km) with a moderate Vp/Vs ratio (~1.76). Although the Ps phase is clearly identifiable, additional energy arrivals at earlier times (~2-3 s) are observed in the radial receiver functions, suggesting the presence of mid-crustal velocity contrasts beneath

Table 1. Geographic coordinates, elevation and H-κ stacking results for the permanent broadband seismic stations used in this study. Crustal thickness (H) and average crustal Vp/Vs ratios represent station-based estimates beneath Eastern Anatolia.

Name	Lat (°)	Lon (°)	Elevation (m)	H (km)	±H (km)	Vp/Vs	±Vp/Vs
BNGB	38.9913	40.6792	1178	40	±1.0	1.64	±0.02
DYBB	37.9532	40.1393	657	38	±1.5	1.69	±0.04
SVAN	38.1511	41.1984	650	37	±1.0	1.69	±0.03
MAZI	37.4593	40.4465	1204	30	±1.5	1.81	±0.04
URFA	37.4409	38.8213	938	34	±1.1	1.69	±0.03
SVRC	38.3775	39.3060	1680	37	±1.3	1.94	±0.03
VRTB	39.1603	41.4558	1498	39	±1.5	1.95	±0.03
YEDI	39.4377	40.5443	1557	40	±1.0	1.76	±0.02
ERZN	39.5867	39.7220	1317	42	±1.0	1.73	±0.02
VANB	38.5090	43.4056	1227	47	±1.5	1.80	±0.04
AGRB	39.5755	42.9920	1820	44	±1.0	1.78	±0.02

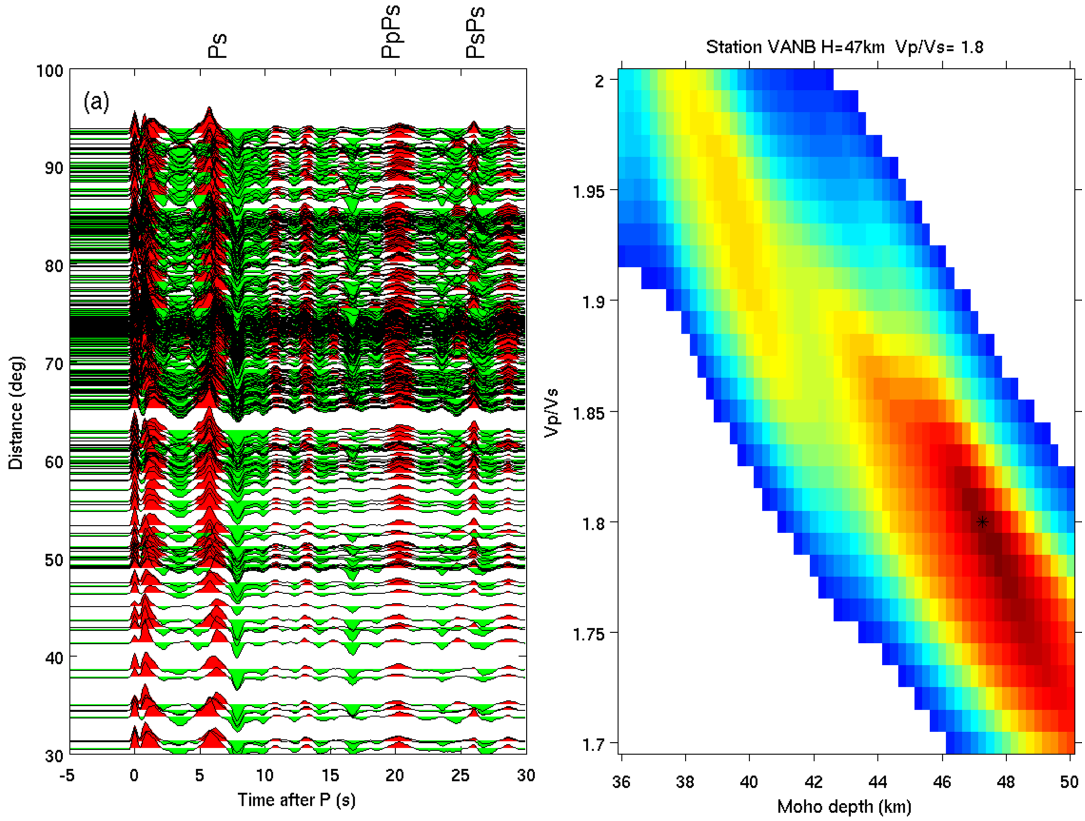

Figure 6. Radial receiver functions at station VANB, sorted by epicentral distance, together with the corresponding H-κ stacking result. Clear Ps and multiple phases indicate a crustal thickness of ~47 km and a Vp/Vs ratio of ~1.80.

the station. Comparable waveform characteristics are also observed at DYBB and SVAN, where moderate crustal thicknesses (~38-39 km) are accompanied by relatively uniform Vp/Vs ratios (~1.69).

At station URFA, the crustal thickness is estimated at approximately 34 km, with a relatively low Vp/Vs ratio (~1.69). Receiver functions at this station display a clear Ps conversion but comparatively weaker crustal multiples, indicating reduced impedance contrasts within the crust.

Uncertainties in the H-κ estimates were evaluated from the width of the high-amplitude regions in the stacking domain and are on the order of ±1.0-1.5 km for crustal thickness and ±0.02-0.04 for Vp/Vs ratios, consistent with previous receiver-function studies in tectonically complex continental regions. All station-based H-κ results are summarized in Table 1.

4. Discussion

4.1 Crustal Thickness Variations beneath Eastern Anatolia

The key advantage of the present dataset lies in its temporal coverage, as it is based on long-term continuous observations processed using a uniform workflow. This enables a more systematic and internally consistent comparison of crustal thickness and Vp/Vs variability across the KTJ region, which is not always possible.

The H-κ stacking results reveal pronounced lateral variations in crustal thickness across Eastern Anatolia, with Moho depths ranging from approximately 30 km to 47 km (Fig. 7). Such a thickened crustal structure is consistent with previous receiver function and seismic tomography studies documenting significant crustal thickening beneath the East Anatolian Plateau (Zor et al., 2003; Angus et al., 2006; Eken et al., 2021; Ogden and Bastow, 2022). For example, Özacar et al. (2010) reported Moho depths of ~33-47 km, while Ogden and Bastow (2022) obtained values of ~34-46 km. This quantitative agreement indicates that the first-order crustal structure resolved in this study is consistent with the established regional framework.

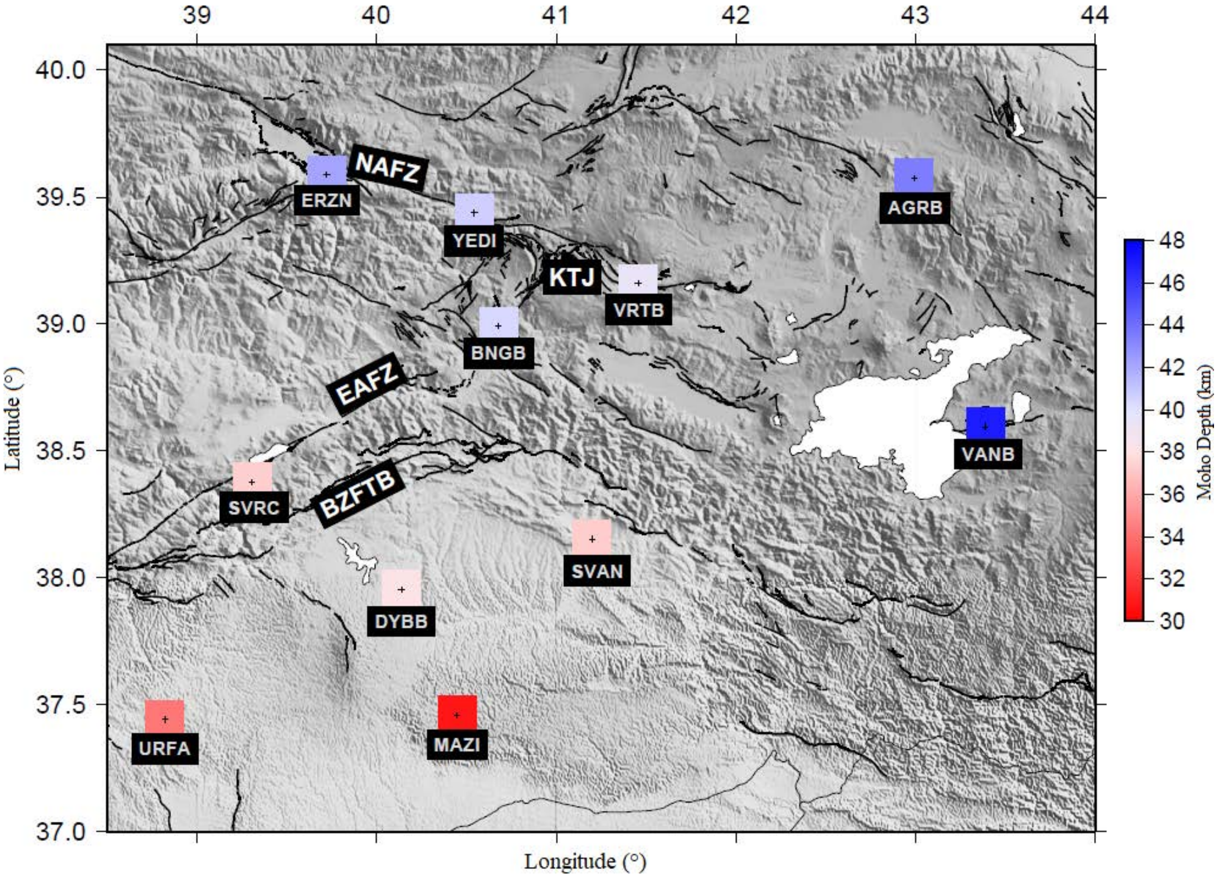

Figure 7. Spatial distribution of crustal thickness (H) derived from H-κ stacking across the KTJ. Faults are shown by solid black lines. Station codes are labelled below the squares. Abbreviations: NAFZ – North Anatolian Fault Zone; EAFZ – East Anatolian Fault Zone; KTJ – Karlıova Triple Junction; BZFTB – Bitlis-Zagros Fold and Thrust Belt.

The thickest crust is observed beneath stations located along or near major active fault zones, particularly in the vicinity of the KTJ and its eastern continuation. This includes stations such as VANB (~47 km) and AGRB (~44 km), which define the maximum crustal thickness in the study area and indicate a general trend of crustal thickening toward the Eastern Anatolian Plateau. Receiver-function characteristics at these stations further support well-resolved Moho depths, with VANB showing a slightly broader stacking response that may reflect local structural complexity, whereas AGRB exhibits a more compact and well-defined solution. This spatial pattern agrees with earlier studies suggesting that crustal thickening in Eastern Anatolia is not uniform, but is instead strongly influenced by tectonic segmentation and strain localization associated with major fault systems (Medved et al., 2021; Güvercin, 2023). Sharp lateral variations in Moho depth near fault junctions have also been reported in migrated receiver function studies, indicating that crustal architecture is significantly shaped by fault-controlled deformation processes (Eken et al., 2021).

Although present-day deformation in Eastern Anatolia is predominantly characterized by strike-slip faulting, the observed crustal thickness values indicate long-term crustal shortening and thickening related to the Arabia-Eurasia continental collision. These processes have been active since at least the Miocene and continue to exert a first-order control on the current crustal structure of the region (Şengör et al., 2003; Le Pichon et al., 2015). Although crustal thickness variations are often broadly associated with surface topography, this relationship is not straightforward in Eastern Anatolia. Previous studies have shown only a weak correlation between Moho depth and elevation (e.g., Ogden and Bastow, 2022), indicating that crustal thickness alone cannot fully explain the observed topography. This is exemplified by station MAZI, located at an elevation of approximately 1200 m, which exhibits a relatively thin crust (~30 km), indicating that crustal thickness alone cannot account for surface elevation and that additional geodynamic processes, including mantle dynamics and thermal structure, likely contribute to the support of the East Anatolian Plateau (Şengör et al., 2003; Faccenna and Becker, 2010; van Hinsbergen et al., 2024).

The observed crustal thickness variations are also consistent with regional gravity studies documenting widespread negative Bouguer gravity anomalies beneath Eastern Anatolia. These anomalies have been interpreted as reflecting thickened, low-density crust and a thermally modified lithosphere beneath the East Anatolian Plateau (Zor et al., 2003; Gökalp, 2012; Eken et al., 2021). Gravity and isostatic modeling further suggest that the present-day elevation of Eastern Anatolia cannot be explained solely by crustal thickening, but instead requires additional mantle support (Şengör et al., 2003). The combined evidence from receiver function and gravity observations therefore supports a lithospheric structure characterized by reduced density and elevated temperatures beneath the region.

4.2 Interpretation of Vp/Vs Ratios and Crustal Composition

Vp/Vs ratios obtained from H-κ stacking range between 1.64 and 1.99, indicating substantial lateral variations in crustal elastic properties across the study area (Fig. 8). Elevated Vp/Vs ratios (>1.85), observed at stations such as VRTB and SVRC, are consistent with previous studies reporting high Vp/Vs values beneath Eastern Anatolia, particularly in volcanic regions and areas affected by high thermal gradients (Zandt and Ammon, 1995; Christensen, 1996; Keskin, 2003; Eken et al., 2021).

High Vp/Vs ratios are commonly interpreted as indicative of mafic lower-crustal compositions, elevated temperatures and/or the presence of partial melt or crustal fluids (Christensen, 1996; Zandt and Ammon, 1995). In Eastern Anatolia, such interpretations are supported by widespread Neogene-Quaternary volcanism and multiple geophysical observations suggesting a thermally weakened lithosphere (Keskin, 2003; Gök et al., 2007; Faccenna and

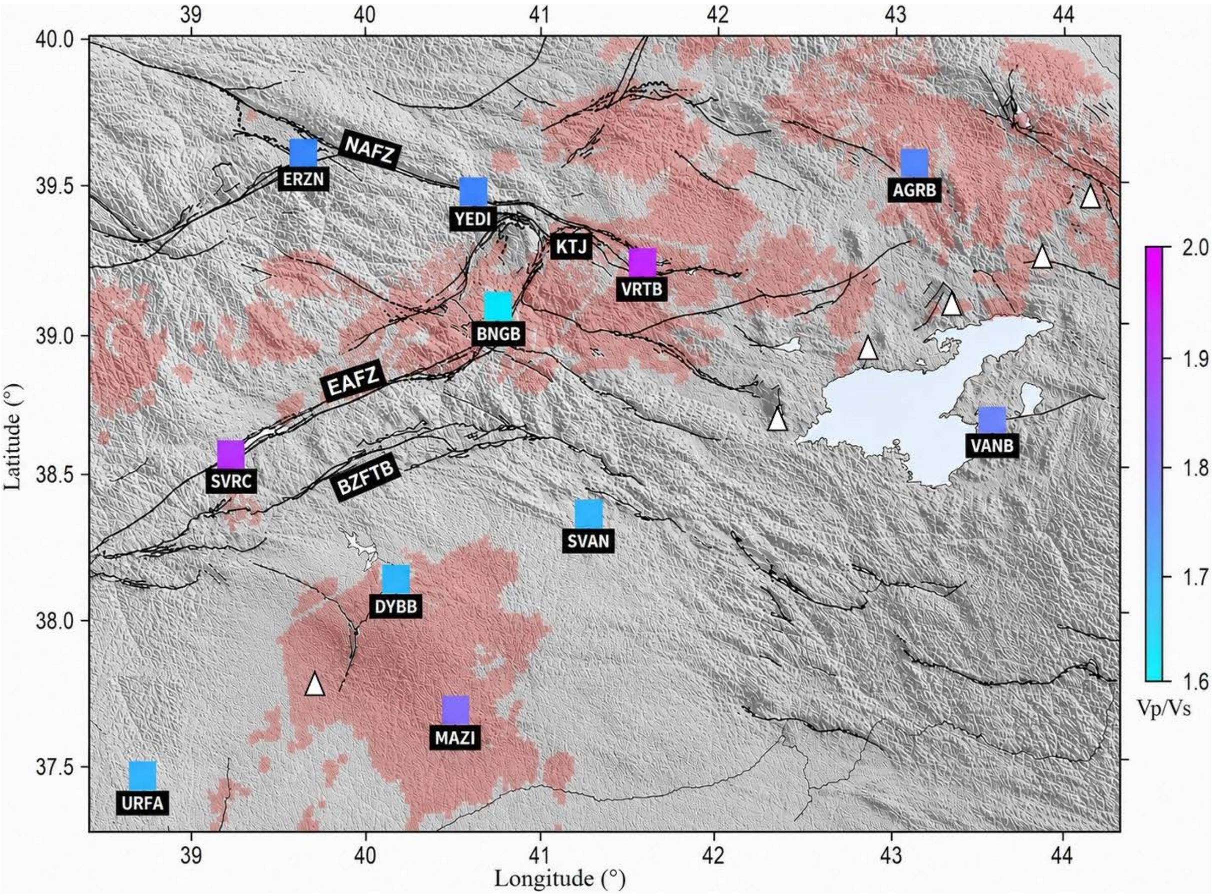

Figure 8. Spatial distribution of crustal Vp/Vs ratios derived from H-κ stacking across the KTJ. Faults are shown by solid black lines, Neogene Quaternary volcanic units are indicated by shaded pink areas and Holocene volcanoes are shown by white triangles. Station codes are labelled below the squares. The distribution of volcanic units is shown after Ulusoy et al. (2019). Abbreviations: NAFZ – North Anatolian Fault Zone; EAFZ – East Anatolian Fault Zone; KTJ – Karlıova Triple Junction; BZFTB – Bitlis-Zagros Fold and Thrust Belt.

Becker, 2010). In contrast, stations exhibiting lower Vp/Vs ratios (≤1.70), such as BNGB and URFA, likely sample relatively more felsic crustal domains or regions with reduced thermal influence. Similar spatial variations in Vp/Vs ratios have been reported by earlier receiver function studies (Zor et al., 2003; Angus et al., 2006). Such variations in Vp/Vs ratios likely reflect spatial differences in crustal composition, fluid content and thermal conditions, pointing to a heterogeneous and dynamically evolving crust beneath Eastern Anatolia.

4.3 Influence of Fault Zones and Structural Segmentation

Stations located directly on or near active fault segments (e.g., ERZN and YEDI) exhibit not only thicker crust but also more complex receiver function waveforms, including additional arrivals at early delay times (~2-3 s). Such waveform characteristics are commonly interpreted as reflecting mid-crustal velocity contrasts or internal crustal layering associated with fault-related deformation and structural heterogeneity (Owens et al., 1984; Cassidy, 1992; Eken et al., 2021). The KTJ represents a particularly complex tectonic environment where strain is transferred between the North and East Anatolian fault systems. Seismic imaging studies have shown that this region is characterized by strong lateral velocity gradients and a segmented crustal architecture, which may exert an important control on earthquake nucleation and rupture propagation (Medved et al., 2021; Cheloni et al., 2025).

The combination of thick crust, elevated Vp/Vs ratios and widespread volcanism supports geodynamic models invoking lithospheric thinning or delamination beneath Eastern Anatolia, resulting in dynamic support of plateau topography (Zor et al., 2003; Faccenna and Becker, 2010; van Hinsbergen et al., 2024).

5. Conclusions

In this study, teleseismic receiver function analysis combined with H-κ stacking was used to investigate crustal thickness and average crustal Vp/Vs ratios beneath the KTJ-Bingöl region in Eastern Anatolia. Based on the results obtained from permanent broadband seismic stations, the following main conclusions can be drawn:

Pronounced lateral variations in crustal thickness are observed across the study area, with Moho depths ranging from approximately 30 km to 47 km. Stations located along or near major active fault zones generally exhibit thicker crust compared to stations situated farther from the fault systems, highlighting strong spatial heterogeneity in crustal structure.

Vp/Vs ratios show significant variability, ranging between 1.64 and 1.95, indicating marked differences in crustal elastic properties. Elevated Vp/Vs ratios are predominantly observed at stations located near active fault zones and in areas associated with Neogene-Quaternary volcanism, whereas lower values characterize comparatively less modified crustal domains. This spatial pattern suggests that the observed Vp/Vs variability reflects differences in crustal elastic properties related to lateral changes in crustal composition, structural complexity, and thermal conditions across Eastern Anatolia.

Receiver-function waveforms reveal clear Ps conversions and well-developed crustal multiples at most stations, confirming the robustness of the H-κ solutions. At several stations, additional arrivals at earlier delay times suggest the presence of mid-crustal velocity contrasts, reflecting internal crustal complexity.

The combined patterns of crustal thickness, Vp/Vs ratios and receiver-function characteristics indicate that the crust beneath Eastern Anatolia is laterally heterogeneous and cannot be represented by a laterally uniform crustal model. The observed combination of thicker crust, elevated Vp/Vs ratios and locally complex receiver-function waveforms, particularly near major fault zones and areas associated with Neogene-Quaternary volcanism, suggests that crustal structure in the region is shaped by the combined effects of tectonic segmentation, active faulting, and regionally variable thermal conditions.

The results provide a consistent basis for interpreting crustal structure and its relationship to major fault systems in Eastern Anatolia. They may also contribute to the broader understanding of large earthquake processes in the region, including recent events such as the 2023 Kahramanmaraş earthquake sequence.

Statements and Declarations Funding. The author declares that no funds, grants, or other support were received during the preparation of this manuscript.

Competing Interests. The author declares that she has no relevant financial or non-financial interests to disclose.

Author Contributions. The author solely contributed to the conception and design of the study, data analysis, interpretation of the results and writing of the manuscript.

Data Availability Statement. The seismic waveform data used in this study are publicly available through the Kandilli Observatory and Earthquake Research Institute (KOERI) data services and through the EIDA portal. https://eida.koeri.boun.edu.tr/webinterface/

References

Al-Lazki, A. I., D. Seber, N. Turkelli, R. Mohamad et al. (2003). Tomographic Pn velocity and anisotropy structure beneath the Anatolian Plateau (eastern Turkey) and surrounding regions, Geophys. Res. Lett., 30, 24, 8046, doi:10.1029/2003GL017391.

Ambraseys, N. N. and J. A. Jackson (1998). Faulting associated with historical and recent earthquakes in the eastern Mediterranean region, Geophys. J. Int., 133, 2, 390-406, doi:10.1046/j.1365-246X.1998.00508.x.

Angus, D. A., D. C. Wilson, E. Sandvol and J. F. Ni (2006). Lithospheric structure of the Arabian and Eurasian collision zone in eastern Turkey from S-wave receiver functions, Geophys. J. Int., 166, 3, 1335-1346, doi:10.1111/j.1365-246X.2006.03070.x.

Barka, A. A. and K. Kadinsky-Cade (1988). Strike-slip fault geometry in Turkey and its influence on earthquake activity, Tectonics, 7, 3, 663-684, doi:10.1029/TC007i003p00663.

Barka, A. and R. Reilinger (1997). Active tectonics of the eastern Mediterranean region deduced from GPS, neotectonics and seismicity data, Ann. Geophys., 40, 587-610, doi:10.4401/ag-3892.

Bayrak, E., Ş. Yılmaz, M. Softa and T. Türker et al. (2015). Earthquake hazard analysis for East Anatolian Fault Zone, Turkey, Nat. Hazards, 76, 2, 1063-1077, doi:10.1007/s11069-014-1541-5.

Bektaş, Ö., A. Pirti, H. Alkan, M. A. Yücel et al. (2025). Stress accumulation on the Karlıova (Bingöl) Triple Junction after two large earthquakes (Pazarcık-Ekinözü) in Türkiye in 2023, Bull. Geophys. Oceanogr., 66, 1-22, doi:10.4430/bgo00485.

Beltran, L., E. A. Bergman, M. D. Cambaz, É. Gaudreau et al. (2020). The 2020 Mw 6.8 Elazığ (Turkey) earthquake reveals rupture behavior of the East Anatolian Fault, Geophys. Res. Lett., 47, e2020GL088136, doi:10.1029/2020GL088136.

Bozkurt, E. (2001). Neotectonics of Turkey-a synthesis, Geodin. Acta, 14, 3-30, doi:10.1016/S0985-3111(01)01066-X.

Cassidy, J. F. (1992). Numerical experiments in broadband receiver function analysis, Bull. Seismol. Soc. Am., 82, 3, 1453-1474, doi:10.1785/BSSA0820031453.

Cheloni, D., N. A. Famiglietti, A. Akinci, R. Caputo et al. (2025). Modeling the 2023 Türkiye earthquakes and strain accumulation along the East Anatolian Fault Zone: Insights from InSAR, GNSS and small-magnitude seismicity, with implications for the seismic potential at rupture terminations, Remote Sens., 17, 13, 2270, doi:10.3390/rs17132270.

Christensen, N. I. (1996). Poisson's ratio and crustal seismology, J. Geophys. Res. Solid Earth, 101, B2, 3139-3156, doi:10.1029/95JB03446.

Colavitti, L., D. Bindi, G. Tarchini and D. Scafidi (2025). A high-quality data set for seismological studies in the East Anatolian Fault Zone, Türkiye, Earth Syst. Sci. Data, 17, 3089-3108, doi:10.5194/essd-17-3089-2025.

Eken, T., M. T. Qashqai, C. Schiffer, T. Taymaz et al. (2021). New insights into crustal properties of Anatolia and its surroundings inferred from P-coda autocorrelation inversions, J. Geophys. Res. Solid Earth, 126, e2021JB023184, doi:10.1029/2021JB023184.

Faccenna, C. and T. W. Becker (2010). Shaping mobile belts by small-scale convection, Nature, 465, 602-605, doi:10.1038/nature09064.

Gök, R., E. Sandvol, N. Türkelli, D. Seber et al. (2003). Sn attenuation beneath the Anatolian Plateau, Geophys. Res. Lett., 30, 24, 8045, doi:10.1029/2003GL017532.

Gök, R., I. D. Bastow, R. Kounoudis, C. S. Ogden et al. (2007). Lithospheric structure of the Anatolian Plateau from surface wave tomography, J. Geophys. Res. Solid Earth, 112, B07301, doi:10.1029/2006JB004689.

Gökalp, H. (2012). Tomographic imaging of the seismic structure beneath the East Anatolian Plateau, Eastern Türkiye, Pure Appl. Geophys., 169, 10, 1749-1776, doi:10.1007/s00024-011-0432-x.

Gülerce, Z., S. T. Shah, A. Menekşe and A. A. Özacar et al. (2017). Probabilistic Seismic-Hazard Assessment for East Anatolian Fault Zone Using Planar Fault Source Models, Bull. Seismol. Soc. Am., 107, 5, 2353-2366, doi:10.1785/0120170009.

Güvercin, S. E., H. Karabulut, A Ö. Konca, U. Doğan et al. (2022). Active seismotectonics of the East Anatolian Fault, Geophys. J. Int., 230, 50-69, doi:10.1093/gji/ggac045.

Güvercin, S. E. (2023). A local earthquake tomography on the EAFZ shows dipping fault structure, Turk. J. Earth Sci., 32, 294-305, doi:10.55730/1300-0985.1845.

Güvercin, S. E. (2024). The 2023 earthquake doublet in Türkiye reveals the complexities of the East Anatolian Fault Zone: Insights from aftershock patterns and moment tensor solutions, Seismol. Res. Lett., 95, 664-679, doi:10.1785/0220230317.

He, L., G. Feng, W. Xu, Y. Wang et al. (2023). Coseismic kinematics of the 2023 Kahramanmaras, Turkey earthquake sequence from InSAR and optical data, Geophys. Res. Lett., 50, e2023GL104693, doi:10.1029/2023GL104693.

Jackson, J. and D. McKenzie (1988). The relationship between plate motions and seismicity, Rev. Geophys., 26, 317-334, doi:10.1029/RG026i002p00317.

Jolivet, L. and C. Faccenna (2000). Mediterranean extension and slab dynamics, Tectonics, 19, 1095-1106, doi:10.1029/2000TC900018.

Karabulut, H., A. Paul, A. D. Özbakir, T. Ergün et al. (2019). A new crustal model of the Anatolia-Aegean domain: evidence for the dominant role of isostasy in the support of the Anatolian plateau, Geophys. J. Int., 218, 57-73, doi:10.1093/gji/ggz147.

Karabulut, H., S. E. Güvercin, J. Hollingsworth and A. Ö. Konca (2023). Long silence on the East Anatolian Fault Zone (Southern Turkey) ends with devastating double earthquakes (6 February 2023) over a seismic gap: implications for the seismic potential in the Eastern Mediterranean region, J. Geol. Soc., 180, doi:10.1144/jgs2023-021.

Keskin, M. (2003). Magma generation by slab steepening and breakoff beneath a subduction-accretion complex: An alternative model for collision-related volcanism in eastern Anatolia, Turkey, Geophys. Res. Lett., 30, 24, 8046, doi:10.1029/2003GL018019.

Konca, A. Ö., H. Karabulut, S. E. Güvercin, F. Eskiköy et al. (2021). From interseismic deformation with near-repeating earthquakes to co-seismic rupture: A unified view of the 2020 Mw6.8 Sivrice (Elazığ) eastern Turkey earthquake, J. Geophys. Res. Solid Earth, 126, e2021JB021830, doi:10.1029/2021JB021830.

Le Pichon, X., A. M. C. Şengör, J. Kende and C. İmren (2016). Propagation of a strike-slip plate boundary within an extensional environment: the westward propagation of the North Anatolian Fault, Can. J. Earth Sci., doi:10.1139/cjes-2015-0129.

Ligorría, J. P. and C. J. Ammon (1999). Iterative deconvolution and receiver-function estimation, Bull. Seismol. Soc. Am., 89, 5, 1395-1400, doi:10.1785/BSSA0890051395.

Liu, C., Y. Yu, G. Liu, C. Pang et al. (2025). The characteristics of seismicity in East Anatolian Fault Zone, Discov. Appl. Sci., 7, 1099, doi:10.1007/s42452-025-07751-2.

McClusky, S., S. Balassanian, A. Barka, C. Demir et al. (2000). Global Positioning System constraints on plate kinematics and dynamics in the eastern Mediterranean and Caucasus, J. Geophys. Res. Solid Earth, 105, B3, 5695-5719, doi:10.1029/1999JB900351.

McKenzie, D. (1972). Active tectonics of the Mediterranean region, Geophys. J. R. Astron. Soc., 30, 109-185, doi:10.1111/j.1365-246X.1972.tb02351.x.

Medved, I., G. Polat and I. Koulakov (2021). Crustal structure of the Eastern Anatolia region (Turkey) based on seismic tomography, Geosciences, 11, 2, 91, doi:10.3390/geosciences11020091.

Ogden, C. S. and I. D. Bastow (2022). The crustal structure of the Anatolian Plate from receiver functions and implications for the uplift of the central and eastern Anatolian Plateaus, Geophys. J. Int., 229, 1041-1062, doi:10.1093/gji/ggab513.

Owens, T. J., G. Zandt and S. R. Taylor (1984). Seismic evidence for an ancient rift beneath the Cumberland Plateau, Tennessee: A detailed analysis of broadband teleseismic P waveforms, J. Geophys. Res. Solid Earth, 89, B9, 7783-7795, doi:10.1029/JB089iB09p07783.

Özbey, V., S. Ergintav and E. Tan (2024). GNSS Time Series Analysis with Machine Learning Algorithms: A Case Study for Anatolia, Remote Sens., 16, 3309, doi:10.3390/rs16173309.

Pearce, J. A., J. F. Bender, S. E. De Long and W. S. F. Kidd (1990). Genesis of collision volcanism in Eastern Anatolia, Turkey, J. Volcanol. Geotherm. Res., 44, 1-2, 189-229, doi:10.1016/0377-0273(90)90018-B.

Philip, C. A., A. Gvishiani and A. Gorshkov (1989). The Caucasus: an actual example of the initial stages of continental collision, Tectonophysics, 161, 1-21, doi:10.1016/0040-1951(89)90297-7.

Reilinger, R., S. C. McClusky, M. B. Oral, R. W. King et al. (1997). Global Positioning System measurements of present-day crustal movements in the Arabia-Africa-Eurasia plate collision zone, J. Geophys. Res. Solid Earth, 102, B5, 9983-9999, doi:10.1029/96JB03736.

Reilinger, R., S. McClusky, P. Vernant, S. Lawrence et al. (2006). GPS constraints on continental deformation in the Africa-Arabia-Eurasia continental collision zone, J. Geophys. Res. Solid Earth, 111, B05411, doi:10.1029/2005JB004051.

Sandvol, E., N. Turkelli, E. Zor, R. Gok et al. (2003). Shear wave splitting in a young continent-continent collision: An example from eastern Turkey, Geophys. Res. Lett., 30, 24, 8041, doi:10.1029/2003GL017390.

Şengör, A. M. C. (1979). The North Anatolian transform fault: Its age, offset and tectonic significance, J. Geol. Soc., 136, 3, 269-282, doi:10.1144/gsjgs.136.3.0269.

Şengör, A. M. C., S. Özeren, T. Genç and E. Zor (2003). East Anatolian High Plateau as a mantle-supported, north-south shortened domal structure, Geophys. Res. Lett., 30, 24, 8045, doi:10.1029/2003GL017858.

Tan, O., Z. Pabuçcu, M. C. Tapırdamaz, S. İnan et al. (2011). Aftershock study and seismotectonic implications of the 8 March 2010 Kovancılar (Elazığ, Türkiye) earthquake (Mw = 6.1), Geophys. Res. Lett., 38, L11304, doi:10.1029/2011GL047702.

Ulusoy, İ., H. E. Çubukçu, D. Mouralis and E. Aydar (2019). Nemrut Caldera and Eastern Anatolian Volcanoes: Fire in the Highlands, in Landscapes and Landforms of Turkey, C. Kuzucuoğlu, A. Çiner and N. Kazancı (eds), Springer, Cham, 589-599, doi:10.1007/978-3-030-03515-0_35.

van Hinsbergen, D. J. J., T. H. Torsvik, S. M. Schmid, L. C. Maţenco et al. (2024). Orogenic architecture and plateau dynamics of Anatolia, Earth Sci. Rev., 249, 104575, doi:10.1016/j.earscirev.2023.104575.

Wang, B. and S. Barbot (2024). Rupture segmentation on the East Anatolian fault (Turkey) controlled by along-strike variations in long-term slip rates in a structurally complex fault system, Geology, 52, 779-783, doi:10.1130/G52403.1.

Wessel, P., W. H. F. Smith, R. Scharroo, J. Luis et al. (2013). Generic Mapping Tools: Improved version released, Eos Trans. AGU, 94, 45, 409-410, doi:10.1002/2013EO450001.

Zandt, G. and C. J. Ammon (1995). Continental crust composition constrained by measurements of crustal Poisson's ratio, Nature, 374, 152-154, doi:10.1038/374152a0.

Zhu, L. and H. Kanamori (2000). Moho depth variation in southern California from teleseismic receiver functions, J. Geophys. Res. Solid Earth, 105, B2, 2969-2980, doi:10.1029/1999JB900322.

Zor, E., E. Sandvol, C. Gürbüz, N. Türkelli et al. (2003). Crustal structure of the Anatolian Plateau from receiver function analysis, Geophys. Res. Lett., 30, 80444, doi:10.1029/2003GL018192.

***CORRESPONDING AUTHOR: Tuğçe ERGÜN**,
Boğaziçi University, Kandilli Observatory and Earthquake Research Institute,
Regional Earthquake-Tsunami Monitoring Center, İstanbul, Türkiye
e-mail: afacan@bogazici.edu.tr